Fuschini et al. EURASIP Journal on Wireless Communications and Networking (2016) 2016:4
DOI 10.1186/s13638-015-0502-3

EURASIP Journal on Wireless Communications and Networking
a SpringerOpen Journal

RESEARCH Open Access

Item level characterization of mm-wave indoor propagation

F. Fuschini[1*], S. Häfner[2], M. Zoli[1], R. Müller[2], E. M. Vitucci[1], D. Dupleich[2], M. Barbiroli[1], J. Luo[3], E. Schulz[3], V. Degli-Esposti[4] and R. S. Thomä[2]

Abstract

According to the current prospect of allocating next generation wireless systems in the underutilized millimeter frequency bands, a thorough characterization of mm-wave propagation represents a pressing necessity. In this work, an "item level" characterization of radiowave propagation at 70 GHz is carried out. The scattering properties of several, different objects commonly present in indoor environment are investigated by means of measurements carried out in an anechoic chamber. The measured data have been also exploited to tune some parameters of a 3D ray tracing model.

Keywords: Millimeter waves, Ray tracing, Measurement, Indoor propagation

1 Introduction

Although first studies on ray tracing (RT) applications to wireless propagation modeling date back to the early 90s [1, 2], RT tools have not received widespread consideration for a long time. In fact, radio system design has been traditionally limited to coverage issues, and empirical/statistical models (such as the Hata formulas [3]) have usually represented the best solution to provide narrowband, path loss (PL) predictions with average accuracy similar to RT approaches but with a much lower complexity and computational demand.

Things have started changing with the massive advent of multi-antenna solutions (MIMO), already included in the 802.11ad and 4G (LTE) standards, and also considered for the future 5G systems [4–6], where system performance is still dependent on the received signals strength but also on parameters related to the multipath richness of the propagation environment (angular/temporal dispersion, multipath correlation coefficients, etc.). The unsuitability of simple narrowband empirical/statistical models for the assessment of such parameters has somehow spurred to resort to ray tracing techniques, which can naturally model the main multipath effects affecting the performance of MIMO systems [7]. Lately, the increasing interest in RT models is being also stimulated by the ongoing idea of allocating next generation wireless systems in the millimeter-wave bands to cope with the unceasing demand for higher data rates [3, 5], since of course the higher the operating frequency, the more accurate the ray-optics approximations. Moreover, due to the technological evolution, computational resources available to radio wave engineers can be expected to become greater and cheaper in the future, contributing to overcome traditional high-CPU time limitations [8].

In this framework, several studies [9, 10] highlighted that wideband and multidimensional prediction capability can be strongly improved if the RT prediction is somehow extended to diffuse scattering (DS or dense multipath component (DMC)), i.e. to the multitude of multipath micro-contributions arriving at the receiver via interactions not included in the specular multipath components (SMC), often with unknown, random phase value and polarization state.

At UHF frequencies, DS can be roughly attributed to the environmental clutter, since both the urban furnishing (outdoor) and the internal furniture (indoor) are often made of objects mainly acting as scatterers rather than reflectors, due to their size comparable to the wavelength or to some surface unevenness and/or volume unhomogeneities. The SMC is on the contrary mainly generated by the "macro-structure" of the propagation scenario represented by walls, floors, and terrain.

* Correspondence: franco.fuschini@unibo.it
[1]Department of Electrical, Electronic and Information Engineering "G. Marconi" (DEI), University of Bologna, IT-40136 Bologna, Italy
Full list of author information is available at the end of the article

According to such distinction, an hybrid empirical/deterministic approach has been proposed, where the SMC is tracked applying the ray-optics rules to a simplified description of the environment (limited to its macrostructure), whereas the DMC is then taken into account by means of an "effective roughness" (ER) approach empirically describing the effects of the clutter not included in the input database [11].

The extension of this analysis to the millimeter frequencies range is somehow questionable and requires further investigations. On the one hand, every object (including walls and floors) appears rougher as the frequency increases; on the other hand, smaller penetration depths are experienced at higher frequencies. The former aspect might contribute to enhance DS due to surface irregularities, whereas the latter may lead to a reduction of the scattering effects related to volume unhomogeneities. Moreover, even small objects commonly not present in the input database may behave as specular reflector at mm-waves due to the smaller wavelength and therefore could contribute also to what we would define SMC [12]. Whether an increase of diffuse scattering must be expected at mm-wave or rather a reduction is an issue still under debate [13]. Hence, multipath interactions at mm-wave could be not simply modeled based on the studies carried out at much lower frequencies. An "item level" characterization of radiowave propagation at mm-wave including scattering from smaller objects is therefore addressed in this work. The scattering properties of several, different objects have been investigated at 70 GHz by means of measurements performed in an anechoic chamber. The measured data have been also exploited to tune some parameters included in a 3D RT model.

One of the purposes of the work is to determine if common indoor objects can be classified into groups having similar scattering characteristics. The final, longer-term goal is to assess whether and how such objects should be taken into account in the description of the propagating scenario in order to get reliable ray tracing predictions at mm-waves.

The paper mainly aims at investigating how the tested items affect mm-wave propagation in terms of penetration loss, polarization coupling, and scattering properties. Moreover, the suitability of a single-lobe scattering model already adopted at lower frequency to describe also mm-wave scattering patterns is discussed. Finally, measurement-simulation comparisons are exploited to improve the accuracy of RT predictions capabilities at mm-frequencies.

The paper is organized as follows: the experimental setup and the ray tracing model to be tuned are shortly described in Sections 2 and 3, respectively. The main outcomes of both the measurement campaign and the RT tuning procedure are outlined in Section 4. Conclusions are finally drawn in Section 5.

2 Experimental setup and measurement description

In order to measure the scattering patterns of different common indoor items (listed in the following Table 1), an ad hoc positioning arrangement has been developed and set up inside an anechoic chamber as shown in Fig. 1.

Measurements have been conducted with the 70 GHz dual-polarized ultra-wideband multichannel sounder (DP-UMCS), developed at Ilmenau University of Technology [14]. It consists of up-/down-converters and an ultra-wideband (UWB) channel sounder based on a M-Sequence radar chip-set [15, 16]. The measurement setup is sketched in Fig. 2.

A single clock generator (fc = 6.75GHz) was used, and the clock signal was distributed to transmitter (Tx) and receiver (Rx) in order to minimize synchronization misalignment. Power amplifiers (PA) were necessary to overcome cable attenuation, in order to have sufficient clock power at Tx and Rx stage.

The UWB stimulus signal is a periodic M-Sequence (spread spectrum signal), generated by 12-stage digital shift register. The impulse response duration is 606 ns and features a bandwidth of 6.75 GHz. According to the sub-sampling frequency of fc/512, a scan rate of about 1600 complex impulse responses per second and per

Table 1 Short description of the OUTs

OUT	W × H × D (cm)	Short description
Brick wall	50 × 50 × 9	Made of hollow bricks and cement, with plaster on external surfaces
PC monitor	45 × 36.8 × 5.8	Squared monitor made of plastic, metal, and glass mix
Bookshelf	43.5 × 32 × 30	Box filled by hardcover books made of cardboard, paper, and small metallic rings
Music speaker	24 × 42 × 21.5	Wooden cabinet with inner speaker cone and ferromagnetic coil
Plant pot	27.3 Ø × 26	Ceramic circular empty pot
Wooden panel	56.5 × 30 × 1.3	Simple plain wood rectangle
Wooden cabinet	56.5 × 30 × 38.1	Heavy plywood locker
Absorber panel	61.5 × 61.5 × 11	Flat-sheet carbon loaded foam absorber

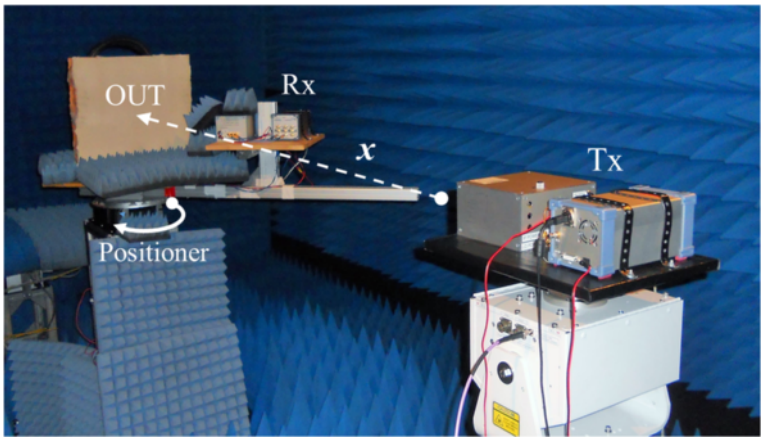

Fig. 1 Anechoic chamber—experimental setup deployed in the anechoic chamber

channel is realized. The frequency range covers the baseband (0 to 3.5 GHz) and FCC-band (3.5 to 10.5 GHz).

Up/down converters are used for mixing the FCC-band and to reach the measurement band of 71–77.75 GHz. A PA at the Tx provides a 1-dB compression point of 30 dBm. In order to avoid saturation effects at the Rx, the transmitting power was attenuated to nearly 0 dBm. Low noise amplifiers (LNA) at the receiver stage feature a gain of 20 dB. Conical horn antennas with approximately 20 dBi gain and 15° half power beam-width (HPBW) were used at the Tx and the Rx stage. It is worth noting that the full 6.75 GHz bandwidth is never reached due to the characteristics of filters and amplifiers at the 70 GHz stage.

Because the DP-UMCS Rx features two receiving channels, two orthogonal polarizations can be measured in parallel. At the Tx, switching between two orthogonal polarizations is conducted. Therefore, the system is capable to measure full polarimetric information.

Basically, each object under test (OUT in the following) was mounted on a rotating plate upon a solid positioner platform scanning all azimuthal angles with 5° step of resolution. The Tx was located in a fixed position 2.21 m apart from the OUT center, whereas the Rx was attached at a distance of 0.408 m on a metallic arm jointly united with the rotational block, thus keeping a constant orientation towards the OUT center (Fig. 3). Both the metallic arm and the receiver module have been covered with absorbing panel, in order to shield as much as possible backscattering contributions not directly coming from the OUT.

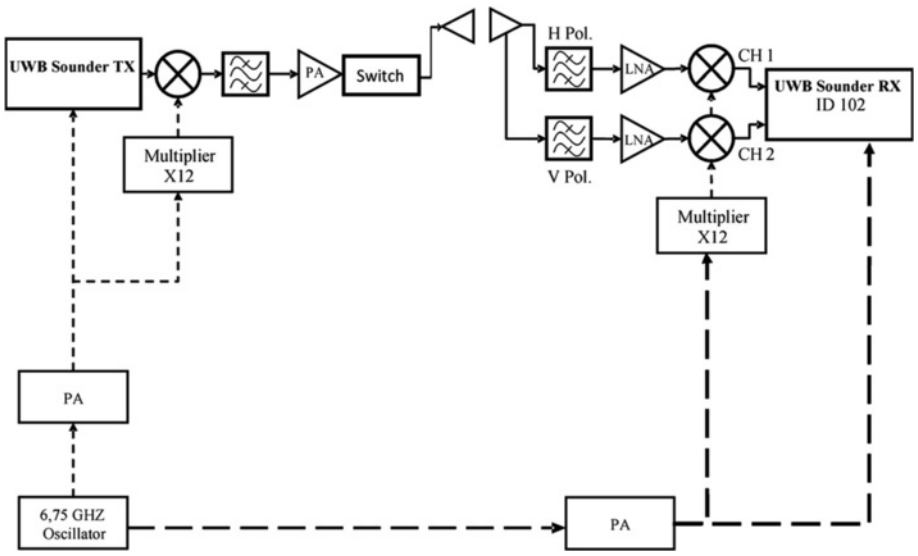

Fig. 2 Channel sounder—block scheme of the channel sounder architecture

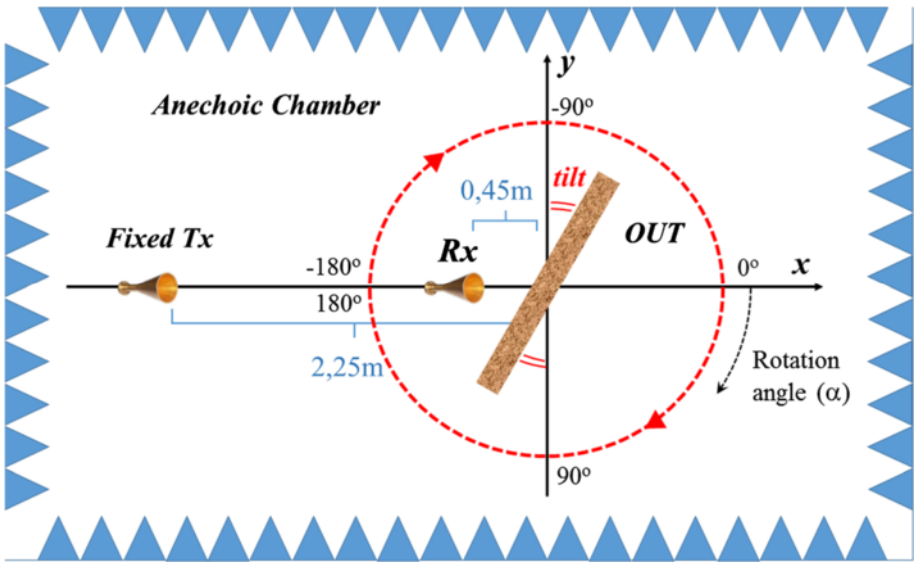

Fig. 3 Measurement setup—overall representation of the measurement setup

For each object, measurements have been repeated with different tilt angles between the Rx and the OUT (Fig. 3), by manually turning the OUT of 0°, 30°, 45°, and 60° over the rotating table.

According to the antenna HPBW value, the Rx-OUT distance has been fixed in order to keep the main radiation footprint well included into the OUT surface, thus reducing possible border effects.

3 Ray tracing model

Simulations have been performed with a 3D Ray Tracing tool (3DScat) specifically conceived for indoor environments and described in detail in [17]. In addition to the coherent interaction mechanisms (reflection, transmission, diffraction) modeled by geometrical optic and uniform theory of diffraction, diffuse scattering is also considered through the effective roughness (ER) approach [11]. In particular, the power density of DS contributions is proportional to a *scattering coefficient* S, related to the overall amount of diffused power, and is modeled according to a *scattering pattern*, describing its spatial distribution. Since DS occurs at the expenses of specular reflection and transmission, a proper reduction factor $R = \sqrt{1-S^2}$ $(0 < R < 1)$ must be applied to reduce reflection/transmission coefficients, in order to preserve the overall power balance [11].

The scattering parameter and the scattering pattern may be in general different in the backward half space (Tx and Rx located on the same side w.r.t. to the considered object) and in the forward half space (Tx and Rx located at opposite sides). Regarding the scattering pattern, several studies have proved that a single-lobe pattern centered on the direction of the specular reflection/transmission is often the best representation [9, 11, 18, 19]. In summary, the power density p of DS in a generic scattering direction can be expressed in the following form [20]:

$$\begin{cases} p(\psi_R) \propto S_R^2 \left(\dfrac{1+\cos\psi_R}{2}\right)^{\alpha_R} \\ p(\psi_T) \propto S_T^2 \left(\dfrac{1+\cos\psi_T}{2}\right)^{\alpha_T} \end{cases} \quad (1)$$

where S_R (S_T) is the scattering coefficient for the backward (forward) half space, ψ_R (ψ_T) is the angle between the reflection (transmission) direction and the scattering direction, and the coefficient α_R (α_T) sets the width of the scattering lobe.

At UHF frequencies, S ranges from 0.2 to 0.4 in rural environment [11], while higher values, up to 0.6, have been estimated in more complex scenarios [19]. Typical values for α range between 2 and 4 [11, 19], allowing to achieve satisfactory prediction accuracy with respect to narrowband and wideband measurement data. However, the reliability of such values also at millimeter frequencies still needs to be fully investigated. With particular reference to indoor scenarios, "forward" scattering may be as important as backscattering to get a complete characterization of the propagation channel. For this reason, the ER model should be parameterized separately in the backward and forward half spaces, following the approach described in [20].

According to the deterministic approach, the RT prediction capability benefits from a detailed description of

the simulation domain. As already discussed, such description is usually limited in indoor environments to walls, floor, and ceiling in order to limit the computational burden and/or because more detailed information are simply unavailable. Nevertheless, the environment representation may be in principle extended also to pieces of furniture or to any other architectural element that can be present inside or outside buildings. For simplicity, in the present work, each object is assumed as made of a finite number of flat-surface slab elements. The geometrical and electromagnetic characteristics are specified in the input files for each wall/object, i.e., vertex coordinates, thickness, complex permittivity, and the parameters of the diffuse scattering model. The 3D polarimetric radiation patterns of Tx and Rx antennas are also required by the RT model.

In order to somehow extend the ER model to the polarization domain, an additional parameter $k_{xpol} \in [0, 1]$ is introduced into the model. Its value basically sets the amount of power transferred into the orthogonal polarization state after a scattering interaction [21]: $k_{xpol} = 0$ means that polarization is perfectly preserved, whereas $k_{xpol} = 0.5$ corresponds to a complete depolarization effect.

4 Analysis of results

Table 1 concisely describes the considered OUT in terms of geometrical dimensions and materials. The list includes a piece of brick wall as the fundamental item involved in almost all indoor and outdoor urban scenarios and a set of rather common objects, usually located in offices or residential premises.

The main properties of the electromagnetic scattering generated by the considered OUT when illuminated by a mm-wave radio signal are investigated in the following sub-sections.

4.1 Analysis of measurement

A summary of the average measured penetration losses for the different objects is reported in Table 2. In agreement with previous studies [4], results confirm that mm-waves undergo higher attenuation with respect to lower frequencies; for example, the comparison between the value in Table 2 and the results shown in [22] suggests that brick wall penetration loss may increase up to a factor 5 if the frequency is moved from 1 to 70 GHz. The PC monitor, probably due to some inner metallic layers and/or components, produces the heaviest obstruction. However, almost all the OUT exhibit a specific attenuation at least equal to ~1 dB/cm.

In order to assess the item impact on signal polarization, the cross-polar discrimination (XPD) values have been extracted from the measured data and are reported in the last column of Table 2. The XPD is defined as the ratio between the received powers in co- and cross-polarized configurations [21]. Without OUT, the XPD is solely determined by antenna cross-polarization isolation (XPI) [23], that is often rather good within the antenna main radiation lobe (23 dB in our case), but it may strongly decrease outside. In order to avoid that the XPD evaluation is shadowed by the poor antenna XPI for some line of sight (LoS) Rx locations, a proper time gating has been therefore applied to the impulsive responses to remove the LoS contribution from the co- and cross-polarized received power values. Despite the propagation delays of the signal contributions coming from the OUT may be very close to the LoS delay for some Rx locations, a sufficient accuracy can be expected on the average due to the excellent time resolution of the measurement equipment (~0.15 ns).

Table 2 Measured obstruction loss and XPD values for the different OUTs

OUT	Obstruction loss (dB)	(dB/cm)	XPD (dB)
None (only antennas)	0	0	23
Brick wall	25.3	2.8	11.7
PC monitor	34.0	5.7	12.7
Bookshelf	30.0	1.0	7.5
Music speaker	18.2	0.85	9.4
Plant pot	16.0	/	10.6
Wooden panel	2.7	2.1	12.8
Wooden cabinet	35.3	0.9	10
Absorber panel	53.8	4.9	4.8

The overall XPD has then been evaluated for each item by averaging over all azimuthal angles and over different OUT tilts.

The XPD for the brick wall is almost 11 dB less than antenna discrimination level, meaning that the item presence introduces an evident de-polarization effect, increasing cross-pol components. This consideration can be extended to all the OUT, since XPD values are always much lower than the antenna XPI.

It is worth noticing that—by definition—the mean XPD values may provide an evaluation of the only overall depolarization effects due to the item presence, without any thorough insight into the corresponding physical reasons, which can be different for the different OUTs. This is for instance highlighted in Fig. 4, where the XPD values are represented against the different antenna positions for the PC monitor and the wooden panel, assuming an OUT tilt equal to 45°.

The monitor XPD is clearly much lower over almost all the forward half-space ($-45° < \alpha < 135°$ in Fig. 4), where transmissions and forward scattering take place. This might be due to the different inner composition of the two OUT, and in particular, the electronic

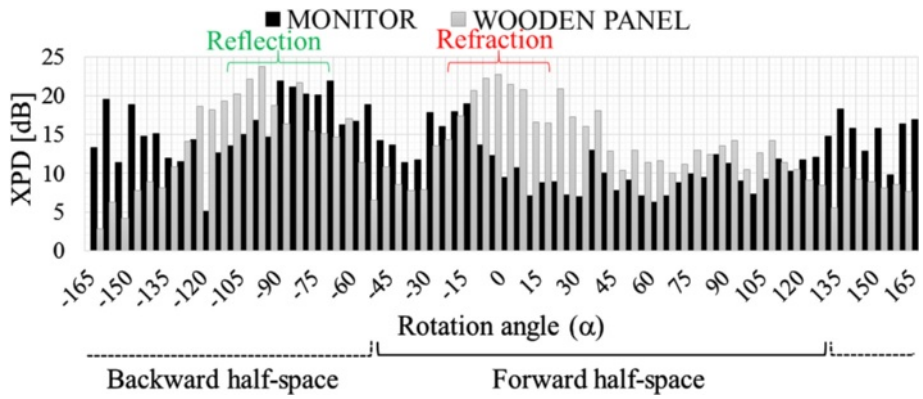

Fig. 4 XPD comparison—comparison between monitor and wooden panel XPD values at 45° tilt angle

components inside the monitor with dimension comparable to λ may produce some de-polarization effects much greater than those determined by the wood fibers of the panel. The situation is basically reversed in the backward half-space ($\alpha > 135^{o}$ and $\alpha < -45^{o}$ in Fig. 4), where reflection and backscattering occur; both the OUT have similar and quite high XPD (>15dB) around the directions of specular reflections (~−90°), whereas far from it the wooden panel exhibit a much lower XPD with respect to the monitor. Apart from specular reflection, backscattering from the wooden panel is mainly caused by its surface roughness; due to its somehow random nature, some cross-polarization coupling can be expected. On the contrary, backscattering from the monitor seems less due to surface roughness (since the screen and the plastic on the rear side appear smoother than the wood surface) and rather determined by signal diffractions on several wedges present especially on the rear side. Since Tx and Rx are placed at the same height, the polarization can be expected unchanged after diffraction on the vertical edges, thus contributing to increase the XPD.

If the XPD values are now averaged over the whole angular range, the differences between the OUTs pointed out in the backward half-space are somehow counterbalanced by those in the forward half-space and similar overall XPD are therefore achieved. As argued, this does not mean the PC monitor and the wooden panel affect the polarization of the propagating signal exactly in the same way.

Detailed analyses for the other pairs of OUT are here omitted for the sake of brevity; differences between the tested items, not always fully characterized through the mean XPD values, are better highlighted in Fig. 5, where the XPD cumulative distribution functions (CDF) are represented.

Moreover, the scattering patterns for the different items have also been obtained from the measurement data, as shown in Fig. 6 and Fig. 7 for the VV co-pol. case only. LoS contributions have been again removed, in order to achieve a more reliable representation of the actual scattering patterns.

In particular, the absolute received powers over the entire angular range [−180°,+175°] for the brick wall in different tilt angles configurations are shown in Fig. 6: there are lobes around the reflection angles, around +120° for 30° tilt, +90° for 45° tilt, and +60° for 60° tilt, respectively. The main effect of backward diffuse scattering is seized in the angular width of the lobes, always equal nearly to 20°. Looking at the angles from 0° to 90°, evident transmissions lobes are clearly not present and forward scattering appears rather uniformly distributed in space. A possible explanation may refer to the volume unhomogeneities represented by the brick structure holes, which could contribute to scatter the energy as the wave penetrates the wall.

The scattering patterns of some OUT are compared in Fig. 7. It is evident that the wooden panel behaves rather differently from the others OUT, since it exhibits the narrower radiation lobe in the backward half-space and is the only item showing a clear scattering lobe also in the forward half-space. This seems rather consistent with its physical properties: despite a slight surface roughness and some inner unhomogeneities represented by the wood fibers that might be perceived at mm-frequencies due to the small wavelength, the wooden panel seems in fact the smoother and the more homogeneous among the considered OUT.

The monitor shows a somehow opposite behavior, with a radiated power rather widespread over the whole spatial domain. Of course, the overall amount of scattered power is much less in the forward half-space, due to the large obstruction loss. Such power spatial distribution is likely due to both the surface irregularities (especially on the rear side) and the internal volume unhomogeneities.

The brick wall behavior is in between the wooden panel and the monitor, may be more similar to the

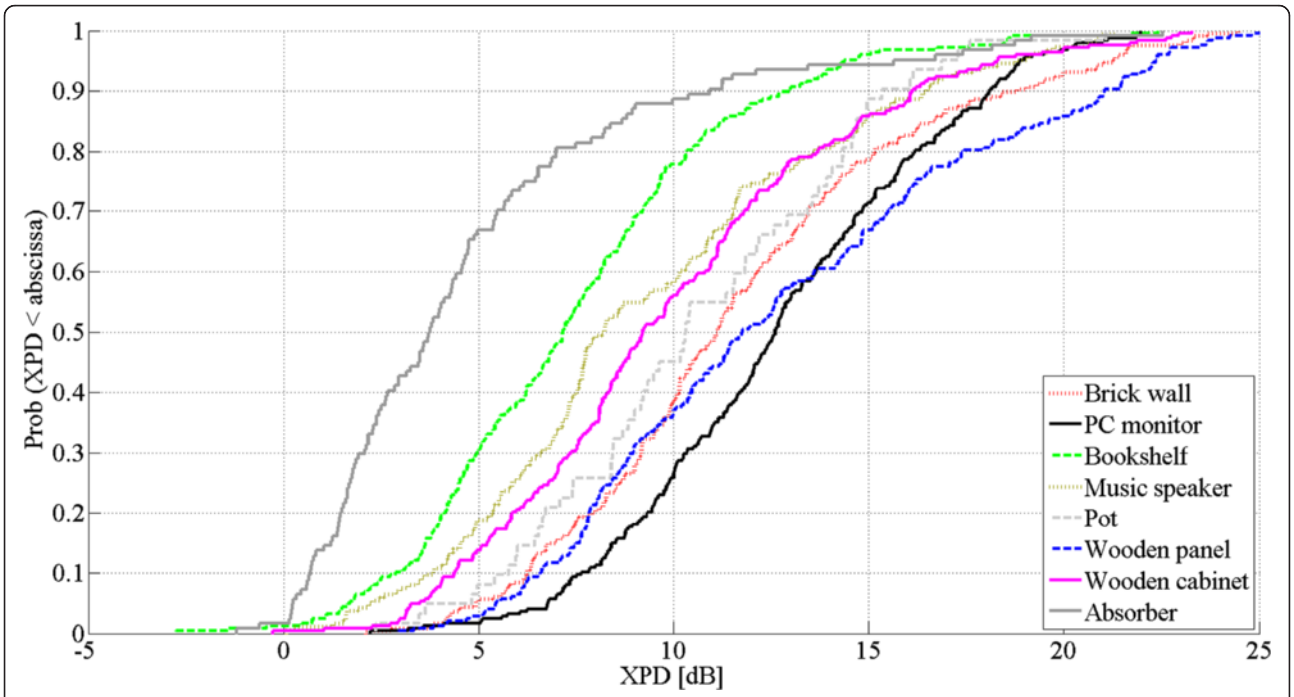

Fig. 5 XPD CDFs—comparison between XPD CDFs of the different items

former in the backward half-space and on the contrary closer to the latter in the forward one.

A widespread scattering pattern in space does not necessarily involve a major cross-polarization coupling produced by the item. In fact, the PC monitor and the wooden panel have rather different scattering patterns (Fig. 7) and similar mean XPD values at the same time (Table 2).

Finally, the plant pot (yellow color) does not exhibit any flat surface offering no specular peaks but rather an almost omnidirectional scattering pattern.

Depending on the type of material, the size and the shape of the OUT and the spatial distribution of the scattered power, together with the polarization properties of the scattered field, may therefore vary accordingly, becoming somehow item-dependent features.

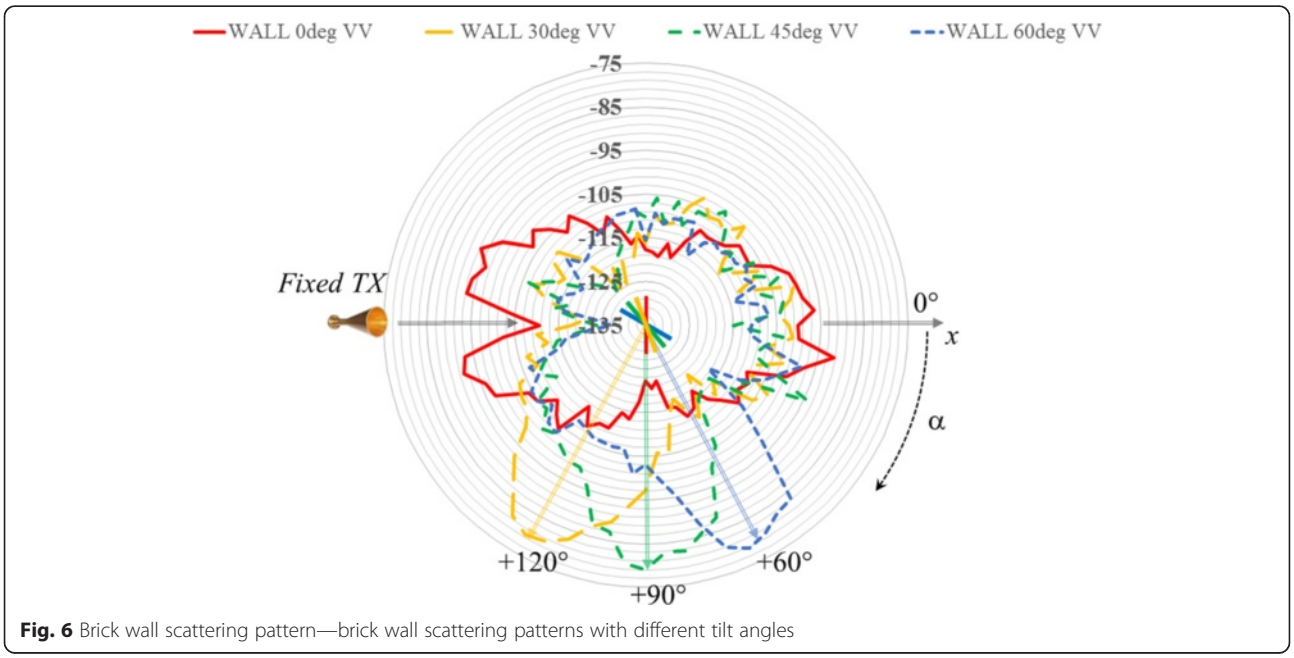

Fig. 6 Brick wall scattering pattern—brick wall scattering patterns with different tilt angles

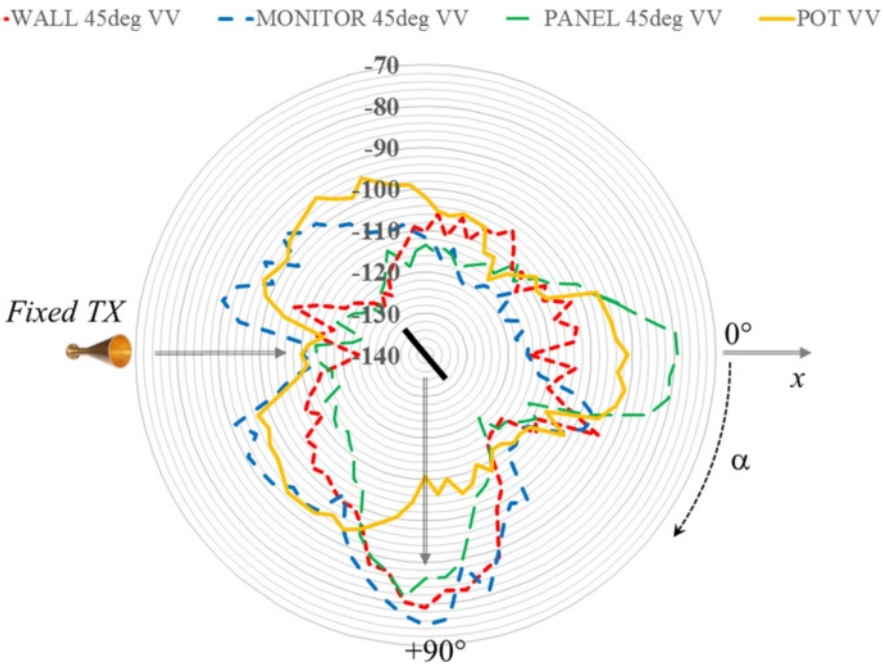

Fig. 7 Scattering patterns for the different OUT—scattering patterns at 45° tilt angle for the different OUT

4.2 RT parameters tuning

The analysis of the measurement data suggests that the backscattered field intensity on the average decreases as the angular distance from specular reflection increases (Fig. 7); furthermore, this behavior is shared by almost all the OUT. Therefore, the single-lobe scattering model described by Eq. 1 and validated at UHF frequencies in several previous studies [11] seems still rather reliable also at mm-wave to account for item backscattering. With reference to forward scattering, the model performance seems poorer and more item-dependent. Preliminary investigation in fact suggests that depending on the amount of inner unhomogeneities, the forward scattered power can be still mainly radiated around the direction of refraction or on the contrary almost uniformly distributed in space (Fig. 7). Although the single lobe model may not represent in the latter case the best approximation, it is still adopted here, and this section is therefore devoted to tune the model parameters based on the experimental characterization.

According to [21], the depolarization parameter k_{xpol} of the DS model embedded into the RT tool has been related to the XPD measured values achieved for the different OUT through the following expression:

$$k_{\mathrm{xpol}} = \frac{1}{1 + 10^{\mathrm{XPD}/10}} \tag{2}$$

It is worth noticing that DS is here intended as any signal contribution not tracked by "standard" RT tool basically because of the limited and (over)simplified description of the items in the input database. In practice, since objects are usually described as made of flat and smooth slab elements, conventional RT models are limited to reflection and refraction from flat, smooth, and homogeneous interfaces, plus diffraction from the border. The ER model aims therefore at modeling everything else.

The XPD values to be included in Eq. (2) have been therefore computed excluding the Tx locations close to the reflection/refraction directions (as already discussed at the end of Section 2, diffraction from the border is assumed negligible since the footprint of the Rx antenna is well included into the OUT surface). The corresponding k_{xpol} values for the considered OUT are listed in the first column of Table 3.

As for the mean XPD values in Table 2, a thorough comprehension of the achieved k_{xpol} values in Table 3 would require a rather detailed analyses. If the PC monitor is for instance considered, the contribution of diffraction to the scattering pattern far from reflection and refraction directions may be rather important; since diffraction undergoes a limited cross-polarization coupling, this may contribute to explain why the monitor is associated with the lowest k_{xpol} value in Table 3. Different OUTs, like the brick wall or the wooden panel, have a scattering pattern mainly determined by distributed surface roughness (at least in the backward half-space), and this may explain their corresponding larger k_{xpol} values.

K_{xpol} estimates in Table 3 are lower than the values presented in [24], where k_{xpol} up to 0.5 has been found

Table 3 Suggested values and ranges for the electromagnetic and scattering parameters achieved through the RT-based tuning procedure

OUT	k_{xpol}	ε_R	σ	S_R	α_R	S_T	α_T
Brick wall	0.13	4–8	0.2–0.4	0.2–0.4	2.6–5.4	0.4–0.9	2.3–5.1
PC monitor	0.07	8–16	0.5–1	0.5–0.8	2.1–4.9	0.6–0.9	2–4.6
Bookshelf	0.2	2–3	0.05–0.8	0.2–0.6	2.6–5.4	0.4–0.9	2.5–5.3
Music speaker	0.23	9–19	0.1–0.2	0.3–0.5	2.8–5.6	0.3–0.7	2.4–5.3
Plant pot	0.1	–	–	–	–	–	–
Wooden panel	0.14	2–4	0.1–0.5	0–0.25	2.7–5.5	0.1–0.3	2.6–5.5
Wooden cabinet	0.13	2–10	0.1–0.2	0.15–0.25	2.8–5.6	0.2–0.7	2.6–5.4
Absorber panel	0.28	2–8	0.4–1.2	0–0.2	2.5–5.4	0.2–0.8	2.6–5.4

at 3.8 GHz. Nevertheless, the analyses carried out in [24] are related to real office/urban environments where the propagating waves may undergo multiple interactions, whereas here multipath propagation is basically limited to a single bounce. Assuming that the wave depolarization on the average increases with the number of undergone interactions, the k_{xpol} values listed in Table 3 can therefore represent a lower bound in a very simple scenario, useful to distinguish contribution of a single object. These single contributions may be composed together to obtain the value of k_{xpol} in more complex scenarios, made of multiple items. .

In order to tune also the remaining parameters of the ER model ($S_{R/T}$, $\alpha_{R/T}$), the measured received powers for the different rotation angles have been compared with the corresponding predictions provided by the 3D RT tool shortly introduced in Section 3. RT simulations have been repeated for different values of the scattering parameters (S_R, α_R, S_T, and α_T), and the root mean square error (RMSE) has been then computed over all the rotation angles for each RT run. Suitable values for the swept coefficients can be at last selected based on the RT simulations with the lower RMSE.

Such approach has been also extended to the electromagnetic parameters of the OUT (relative permittivity—ε_R—and electrical conductivity—σ), in order to estimate their values for the OUT never addressed so far (e.g., the monitor or the bookshelf) or to consolidate their evaluation for the most common objects (like the wall sample and the wooden panel), still not reliably and extensively investigated at mm-waves in the few studies available in the literature ([25–27] for a brick wall).

Unfortunately, the narrowband RT results have turned out to be not so sensitive to the electromagnetic and scattering parameters to allow a clear identification of a single optimal value for each of them, since several and sometimes rather different coefficients combinations basically correspond to nearly the same RMSE value. Therefore, in order to find some kind of confidence interval for each coefficient, the better RT runs have been first selected, that is RT simulations corresponding to a RMSE at most 1 dB lower with respect to the best one. Among them, the occurrence of each tested value for each RT parameter has been then computed, thus leading at the end to the identification of the ranges of values with higher probability. The outcome of this outlined procedure is for instance represented in Fig. 8 for the brick wall case and with reference to the only electromagnetic parameters tuning: the most accurate RT predictions correspond to a relative permittivity ranging between 4 and 8, whereas values around 0.3 should be assumed for the electrical conductivity. The complete list of results achieved for all the considered RT parameters and for each OUT is reported in Table 3.

With reference to the electromagnetic parameters, they of course represent in some cases effective values not clearly related to the physical properties of any specific material. This may for instance refer to the monitor and the speaker, which are indeed a compound of many very different materials.

As far as the brick wall is concerned, values of ε_R and σ in Table 3 are not in full agreement with the existing experimental studies, where ε_R values at millimeter frequencies between 2.55 [25] and 4.4 [27] have been found, and σ up to 1.4 S/m has been proposed [25]. A general, rather clear conclusion can be however drawn from the overall different investigations: if compared to the values commonly adopted at UHF frequencies ($\varepsilon_R \approx 5$, $\sigma \approx 10^{-2}$ around 1 GHz [22, 28]), the permittivity value at mm-wave is basically the same, whereas the conductivity is increased by one/two order of magnitude, that is also in agreement with the already discussed increase of the obstruction loss experienced at mm-waves.

With regard to the wooden panel, the achieved ranges for ε_R and σ are fundamentally consistent with the experimental characterization carried out at 60 GHz and described in [25, 29].

If the scattering parameters are now considered, the values gathered in Table 3 reflect the general considerations already outlined at the end of the previous subsection. Since the wooden panel has turned out to be the poorer scatterer among the considered OUT, it is

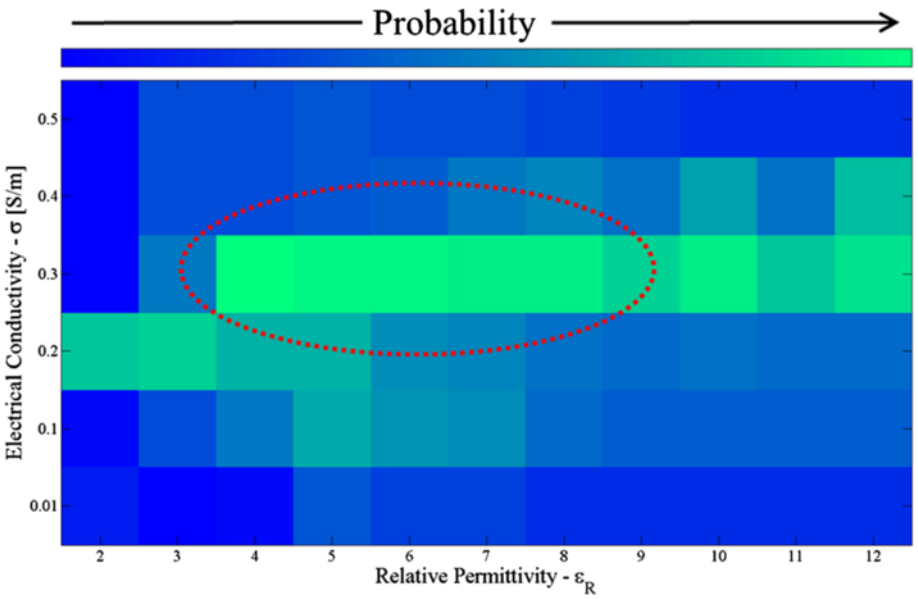

Fig. 8 RT tuning - graphical representation of the outcome of the RT parameters tuning procedure for the brick wall

associated in Table 3 to both the lowest $S_{R/T}$ values and the highest $\alpha_{R/T}$. This actually corresponds to the lower amount of scattered power in the narrower range of spatial directions. On the contrary, the highest $S_{R/T}$ coefficients together with the lowest $\alpha_{R/T}$ values found for the PC monitor can be related with the already mentioned degree of surface irregularities and inner unhomogeneities. The wall sample shows scattering parameters quite similar to the wooden panel in the backward half-space. In particular, S_R ranges between 0.2 and 0.4, i.e, it is slightly larger than the value (0.2) found in [11] for a brick wall at 1.29 GHz. This seems suggesting that scattering might be richer at mm-waves with respect to lower frequencies but to an extent that could be lower if compared to the expectations pointed out in several studies. With regard to the forward half-space, the brick wall behaves instead more similarly to the monitor, and this may be somehow related to the inner unhomogeneities clearly present in both the item structures and on the contrary much less evident within the wooden panel.

All considered, the achieved results seem suggesting that items backscattering is basically determined by the only surface unevenness and not so much by the inner unhomogeneities. OUT like the wooden panel and the brick wall have somehow similar surface properties and share a similar backscattering behavior (i.e., similar S_R and α_R value), although their inner composition is quite different. The small penetration thickness experienced at mm-waves may explain why the scattering in the backward half-space is weakly affected by what is present beyond the item surface.

With reference to the forward half-space, the scattered field is always strongly attenuated due to the high obstruction loss, and a widespread spatial distribution of the scattered power can be noticed in presence of evident volume unhomogeneities.

The overall effectiveness of the procedure carried out to tune the main RT parameters at mm-frequency is finally shown in Fig. 9, where the measured values of the scattered power from the brick wall (tilt = 30°) for different polarization arrangements are compared with the outcomes of two RT simulations, carried out with the tuned parameters values and with the values commonly adopted at UHF frequencies, respectively.

Clearly, simulations carried out with the tuned RT parameters fit the measured data rather well, with RMSE equal to 4.11 and 3.94 dB for the co- and cross-polarized cases, respectively. On the contrary, much poorer accuracy is achieved if the RT is run with the UHF parameters values ($\varepsilon_R = 5$, $\sigma = 10^{-2}$ [22] $S_R = S_T = 0.2$ [11], $k_{\mathrm{xpol}} = 0.05$ [24]), with RMSE increasing up to 9.4 dB (co-pol.) and 5.5 dB (cross-pol.).

With reference to the co-polarized case, the worse performance achieved with the UHF parameters is mainly due to the too low conductivity value, which corresponds to a weaker obstruction loss and therefore to a strong overestimate of the received power over the NLoS region (around 0° in Fig. 9). Minor changes are on the contrary achieved in the backward half-space, since reflection is less sensitive to the conductivity value and therefore is approximately unchanged at the two frequencies. If the cross-polarized case is now considered, the received power is basically due only to diffuse

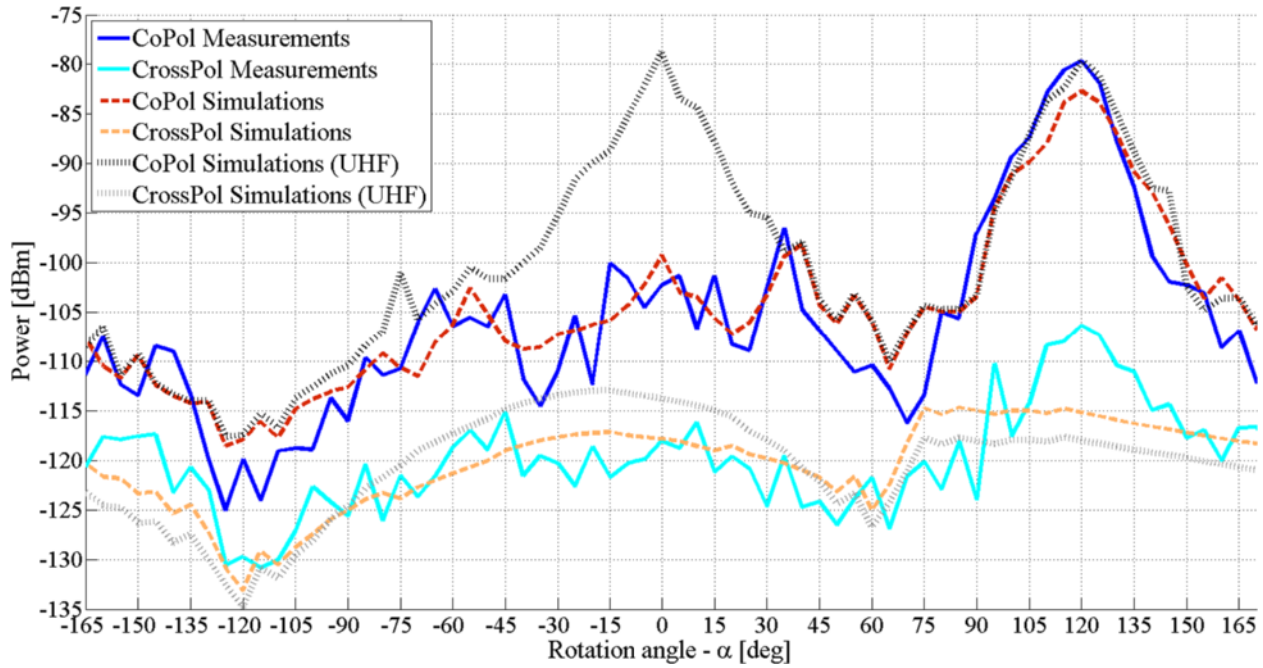

Fig. 9 RT-measurement comparison in co- and cross-polarization—measurement vs simulation prediction in co- ad cross-pol. for the brick wall with a 30° tilt

scattering (because of the non-zero k_{xpol} value), since the coherent contributions carry a negligible power because of the polarization mismatch. With reference to the NLoS locations, the difference between the UHF and the mm-wave case is the result of some different effects: on the one hand, the scattered power at mm-wave is reduced due to the lower amount of transmission; on the other hand, the diffuse scattering at mm-wave is enhanced by the greater scattering coefficient S and the larger k_{xpol} value. Such effects partly counterbalance each other, and this explains the lower power reduction between the two frequency bands in the cross-polarized case with respect to the co-polarized one.

An increase in the received power can be on the contrary observed if the mm-wave case is compared to the UHF result in the backward half-space. Of course, this is due to the greater S value, for (approximately) the same reflected power.

5 Conclusions

In this work, the scattering properties of some different items in the 70 GHz band have been investigated by means of an ultra-wideband channel sounding system with an automatic positioning setup in anechoic chamber. Measurements show quite heavy obstruction losses, as expected at mm-waves, with a specific attenuation approximately ranging from 1 to 6 dB/cm in the considered cases. Penetration losses due to radio wave propagation through a brick wall at 70 GHz may be five times the corresponding value at 1 GHz.

Although average cross-polar discrimination values are not so different, a more detailed analysis suggests that different objects may affect the polarization behavior in a quite different way. In particular, surface roughness as well as inner unhomogeneities seems to foster cross-polarization coupling, that seems on the contrary reduced in presence of sharp, structural protrusions and/or indentations on the item surface.

With reference to the scattering patterns, a backscattering lobe around the direction of specular reflection can be identified for each of the considered items, with an angular amplitude mainly determined by the degree of surface irregularities. On the contrary, a forward scattering lobe cannot be always identified, since the power is often uniformly widespread in the forward half-space, especially in cases where inner unhomogeneities are present.

Measurements have been then used to calibrate a RT tool at mm-waves, and in particular to tune both the electromagnetic characteristics of different objects and the main parameters of the single-lobe, diffuse scattering model embedded in the simulator. With reference to the brick wall as the most common—and therefore rather interesting—object, the permittivity at mm-wave is basically quite similar to what is found at UHF frequencies, whereas the conductivity is increased by one/two order of magnitude. Moreover, backscattering from a brick wall seems richer at mm-waves than at lower

frequencies but to a lower extent than what suggested in several previous studies.

Future work will assess the RT prediction capabilities at mm-waves in real, multi-object scenarios, and in particular whether an item level description of the propagation environment is really necessary to achieve reliable predictions.

Competing interests
The authors declare that they have no competing interests.

Author details
[1]Department of Electrical, Electronic and Information Engineering "G. Marconi" (DEI), University of Bologna, IT-40136 Bologna, Italy. [2]Ilmenau University of Technology, 98684 Ilmenau, Germany. [3]European Research Center, Huawei Technologies Duesseldorf GmbH, 80992 Munich, Germany. [4]Polariss Wireless Inc., Mountain View, CA 94043, USA.

Received: 31 July 2015 Accepted: 20 December 2015
Published online: 06 January 2016

References

1. JW Mckown, RL Hamilton, Ray tracing as a design tool for radio networks. IEEE Network Magazine **5**, 27–30 (1991). doi:10.1109/65.103807
2. JP Rossi, JC Bic, AJ Levy, Y Gahillet, M Rosen, APS'91: A ray launching method for radio-mobile propagation in urban area, IEEE Int. Symposium on Antennas and Propagation Digest. **3**, 1540-1543. doi: 10.1109/APS.1991.175146
3. M Hata, Empirical formula for propagation loss in land mobile radio services. IEEE Trans on Vehicular Tech **29**(3), 317–325 (1980). doi:10.1109/T-VT.1980.23859
4. TS Rappaport, S Sun, R Myzus, H Zhao, Y Azar, K Wang, GN Wong, JK Schulz, M Samimi, F Gutierrez, Millimeter wave mobile communication for 5G cellular: it will work! IEEE Access **1**, 335–349 (2013). doi:10.1109/ACCESS.2013.2260813
5. W Roh, J-Y Seol, J Park, B Lee, J Lee, Y Kim, J Cho, K Cheun, F Aryanfar, Millimeter-wave beamforming as an enabling technology for 5G cellular communications: theoretical feasibility and prototype results. IEEE Comm Magazine **52**(2), 106–113 (2014). doi:10.1109/MCOM.2014.6736750
6. W Hong, K-H Baek, Y Lee, Y Kim, S-T Ko, Study and prototyping of practically large-scale mmWave antenna systems for 5G cellular device. IEEE Comm Magazine **52**(9), 63–69 (2014). doi:10.1109/MCOM.2014.6894454
7. EM Vitucci, L Tarlazzi, F Fuschini, P Faccin, V Degli-Esposti, Interleaved-MIMO DAS for indoor radio coverage: concept and performance assessment. IEEE Trans on Ant and Propagat **62**(6), 3299–3309 (2014). doi:10.1109/TAP.2014.2313136
8. T Rich. T Kuhlen, Accelerating Radio Wave Propagation Algorithms by Implementation on Graphics Hardware, in Wave Propagation in Materials for Modern Applications, ed. A. Petrin (InTech Publishng), pp. 103-124
9. F Mani, F Quitin, C Oestges, Directional spreads of dense multipath components in indoor environments: experimental validation of a ray tracing approach. IEEE Trans on Ant and Propagat **60**(7), 3389–3396 (2012). doi:10.1109/TAP.2012.2196942
10. F Fuschini, H El-Sallabi, V Degli-Esposti, L Vuokko, D Guiducci, P Vainikainen, Analysis of multipath propagation in urban environment through multidimensional measurements and advanced ray tracing simulation. IEEE Trans Antennas Propagat **56**(3), 848–857 (2008). doi:10.1109/TAP.2008.916893
11. V Degli Esposti, F Fuschini, E Vitucci, G Falciasecca, Measurement and modelling of scattering from building. IEEE Trans on Ant and Propagat **55**(1), 143–153 (2007). doi:10.1109/TAP.2006.888422
12. D Dupleich, F Fuschini, R Müller, EM Vitucci, C Schneider, V Degli Esposti, et al *URSI GASS'14: directional characterization of the 60 GHz indoor-office channel* (IEEE XXXIth URSI General Assembly and Scientific Symposium, Bejing (CH), 2014), pp. 1–4. doi:10.1109/URSIGASS.2014.6929648
13. K Haneda, Channel models and beamforming at millimeter-wave frequency bands. IEICE Trans on Communications **E98B**(5), 755–772 (2015)
14. R Muller, S Hafner, D Dupleich, J Luo, E Schulz, R Herrmann, et al *VTC Spring'15: ultra-wideband channel sounder for measurements at 70 GHz* (IEEE 81st Veh Tech. Conf, Glasgow (SC), 2015), pp. 11–14
15. J Sachs, F Bonitz, M Kmec, M Helbig, R Herrmann, K Schilling, et al Ultra-wideband pseudo-noise sensors. Applied Radio Electronics **12**(1), 79–88 (2013)
16. J Sachs, R Herrmann, M Kmec, Time and range accuracy of short-range ultra-wideband pseudo-noise radar. Applied Radio Electronics **12**(1), 105–113 (2013)
17. F Fuschini, EM Vitucci, M Barbiroli, G Falciasecca, V Degli-Esposti, Ray tracing propagation modeling for future small-cell and indoor applications: a review of current techniques. Radio Sci **50**(6), 469–485 (2015). doi:10.1002/2015RS005659
18. F Mani, F Quitin, C Oestges, Accuracy of depolarization and delay spread predictions using advanced ray-based modeling in indoor scenarios, EURASIP Journal on wireless communications and networking. **11**(1), (2011). doi: 10.1186/1687-1499-2011-11
19. EM Vitucci, F Mani, V Degli-Esposti, C Oestges, Polarimetric properties of diffuse scattering from building walls: experimental parameterization of a ray-tracing model. IEEE Trans Antennas Propagat **60**(6), 2961–2969 (2012). doi:10.1109/TAP.2012.2194683
20. F Fuschini, V Degli-Esposti, EM Vitucci, *EuCAP'10: a model for forward-diffuse scattering through a wall* (4th European Conference on Antennas and Propagation, Barcelona (SP), 2010), pp. 1–4
21. V Degli Esposti, VM Kilomonen, EM Vitucci, P Vainikainen, Analyses and modeling on co- and cross-polarized urban radio propagation for dual polarized MIMO wireless systems. IEEE Trans On Ant And Propagat **59**(11), 4247–4256 (2011)
22. D Pena, R Feick, HD Hristov, W Grote, Measurement and modeling of propagation losses in brick and concrete walls for the 900 MHz band. IEEE Trans on Antennas and Propagation **51**(1), 31–39 (2003)
23. C Oestges, B Clerckx, MIMO wireless networks, 2nd ed. (Elsevier, 2013), p. 76
24. EM Vitucci, F Mani, C Oestges, V Degli Esposti, *ICECom'13: analysis and modeling of the polarization characteristics of diffuse scattering in indoor and outdoor radio propagation* (21st Int. Conf. on Applied Electromagnetics and Communications, Dubrovnik (HR), 2013), pp. 1–5. doi:10.1109/ICECom.2013.6684715
25. J Lu, D Steinbach, P Cabrol, P Pietraski, RV Pragada, *EuCAP'14: propagation characterization of an office building in the 60 GHz band* (8th Eur. Conf. Antennas Propag, The Hague (NL), 2014), pp. 809–813
26. D Ferreira, I Cuinas, RFS Caldeirinha, TR Fernandes, TR Fernandes, *EuCAP'14: a review on the electromagnetic characterization of building materials at micro- and millimetre wave frequencies* (8th Eur. Conf. Antennas Propag, The Hague (NL), 2014), pp. 145–149
27. I Cuinas, J-P Pugliese, A Hammoudeh, MG Sanchez, *VTC Fall'00: comparison of the electromagnetic properties of building materials at 5.8 GHz and 62.4 GHz*, vol. 2 (52nd Veh. Tech. Conf, Boston (MA), 2000), pp. 780–785
28. H L Bertoni, Radio propagation for modern wireless systems, 1st ed. (Prentice Hall, 2000), p. 74
29. LM Correia, PO Frances, *PIMRC'95: transmission and isolation of signals in buildings at 60 GHz*, vol. 3 (6th Int. Symposium on Personal, Indoor and Mobile Radio Communications, Toronto (CDN), 1995), pp. 1031–1034